

Atomic-scale positioning of single spins via multiple nitrogen-vacancy centers

Wen-Long Ma,^{†,‡} Shu-Shen Li,[†] Geng-Yu Cao,[¶] and Ren-Bao Liu^{*,‡,§,||}

State Key Laboratory of Superlattices and Microstructures, Institute of Semiconductors, Chinese Academy of Sciences, Beijing, 100083, China, Department of Physics, The Chinese University of Hong Kong, Shatin, N. T., Hong Kong, China, State Key Laboratory of Magnetic Resonance and Atomic and Molecular Physics, Wuhan Institute of physics and Mathematics, Chinese Academy of Sciences, Wuhan, 430071, China, Center for Quantum Coherence, The Chinese University of Hong Kong, Shatin, N.T., Hong Kong, China, and Institute of Theoretical Physics, The Chinese University of Hong Kong, Shatin, N.T., Hong Kong, China

E-mail: rblu@phys.cuhk.edu.hk

KEYWORDS: nano-magnetometry, nitrogen-vacancy center, spin coherence, dynamical decoupling

Abstract

We present a scheme of positioning a single electron spin with sub-nanometer resolution through multiple nitrogen-vacancy centers in diamond. With unwanted noise suppressed by dynamical decoupling, the spin coherence of each center develops characteristic oscillations

^{*}To whom correspondence should be addressed

[†]State Key Laboratory of Superlattices and Microstructures, Institute of Semiconductors, Chinese Academy of Sciences, Beijing, 100083, China

[‡]Department of Physics, The Chinese University of Hong Kong, Shatin, N. T., Hong Kong, China

[¶]State Key Laboratory of Magnetic Resonance and Atomic and Molecular Physics, Wuhan Institute of physics and Mathematics, Chinese Academy of Sciences, Wuhan, 430071, China

[§]Center for Quantum Coherence, The Chinese University of Hong Kong, Shatin, N.T., Hong Kong, China

^{||}Institute of Theoretical Physics, The Chinese University of Hong Kong, Shatin, N.T., Hong Kong, China

due to a single electron spin located 4~20 nm away from the centers. We can extract the position information from the characteristic oscillations of each center. This scheme is useful for high-resolution nanoscale magnetometry and spin-based quantum computing.

Detection and positioning of single electron spins have important applications in physical, chemical and biological sciences, such as scanning magnetic point defects in solid-state systems,¹ single molecule structural imaging² and tracking individual spin-labels in biological systems.³ Since the magnetic field of a single electron spin is extremely weak, it is difficult to realize nanoscale or atomic-scale resolution in positioning a single spin by conventional magnetic resonance imaging.^{4,5}

The negatively charged nitrogen-vacancy (NV) center⁶⁻⁹ has a paramagnetic spin-triplet ground state that can be optically initialized and read out.^{10,11} The NV center has long spin coherence time up to milliseconds even at room temperature.¹² With recent development in diamond nanofabrication,¹³ the NV center in high-purity diamond has been used as a magnetic sensor to detect single nuclear spins.¹⁴⁻¹⁶ The key idea is to identify the characteristic oscillations caused by the target nuclear spin imprinted onto the NV center spin coherence¹⁷ while suppressing the background noise by dynamical decoupling.^{19,20} However, the position of the target spin cannot be uniquely determined by one experimental setting. Instead, the measurement has to be repeated for various magnetic field orientations to fully position the target spin. Such a requirement restricts the speed of scanning and limits the potential applications in quantum computing.

In this Letter, we propose to use multiple NV centers in a diamond probe tip for positioning single spins with sub-nanometer resolution (1a). This scheme is analogous to the multi-satellite positioning systems. For a given NV sensor spin, the coherent oscillations provide partial information on the distance and direction of the target single spin. The full position information of the target spin can be obtained by the oscillations of the multiple NV center spins. This scheme would greatly improve the speed of detection compared with the scheme using one NV center,¹⁴⁻¹⁷ since there is no need of varying the magnetic field or scanning the probe.^{5,13,18}

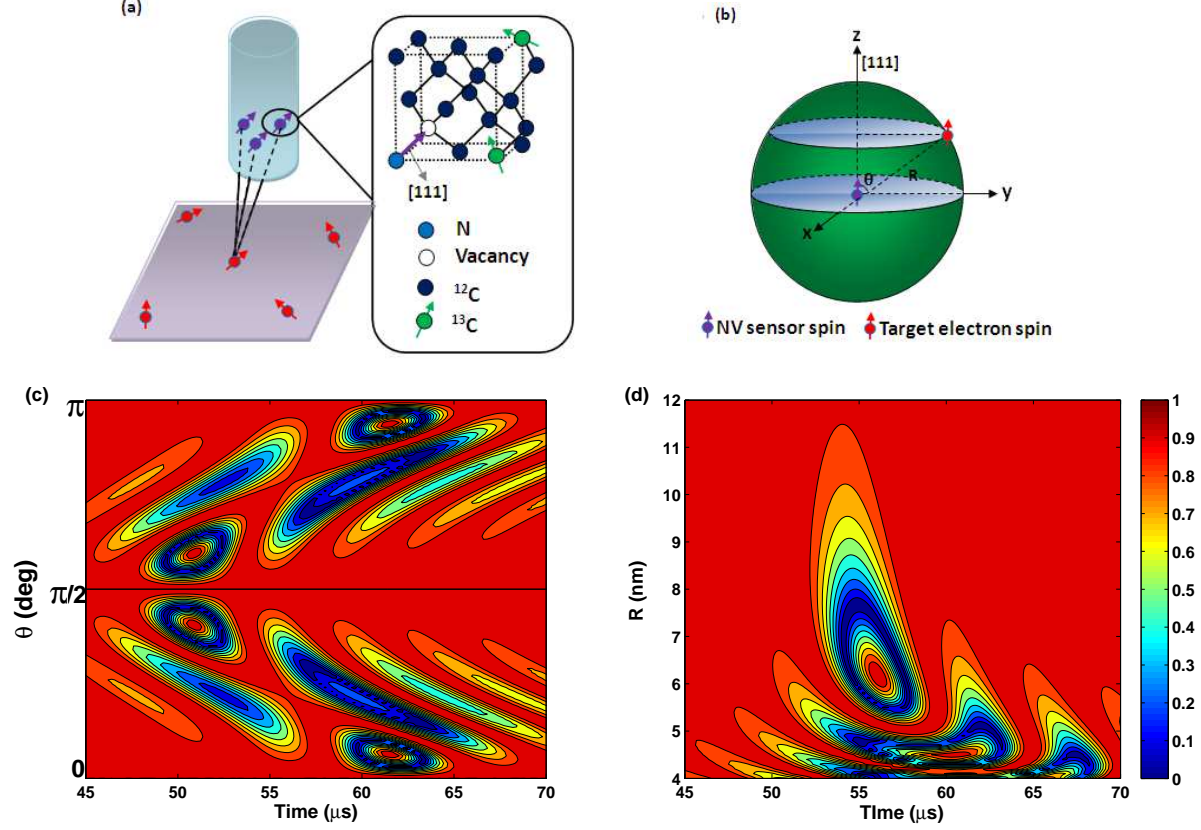


Figure 1: Fingerprint features in NV center spin coherence due to coupling to a single electron spin. (a) Schematic illustration of the single electron spin detection based on three NV centers embedded in a diamond tip. The NV axes of the three NV centers are all along the crystal axis $[111]$. The close-up shows the atomic structure of the NV center. (b) The relative position between a single NV sensor spin and the target electron spin is denoted by the distance R and the zenith angle θ relative to the $[111]$ axis. (c) NV center spin coherence under 30-pulse CPMG control as a function of time and the zenith angle of the target spin at a distance of $R = 5$ nm. (d) NV center spin coherence under 30-pulse CPMG control as a function of time and the distance R of the target spin with a zenith angle $\theta = \pi/6$. The strain-induced transverse anisotropy parameters are $\varepsilon_A = \varepsilon_B = \varepsilon_C = 3$ MHz and a magnetic field $B = 0.1$ Gauss is applied along the NV axis. The calculations for (c) and (d) include only coupling between the NV center and the target spin (the nuclear spin bath not considered).

The full Hamiltonian of the whole system is written as

$$H = H_{target} + \sum_i H_{NV_i} + H_{bath} + \sum_{i,j} H_{NV_i-NV_j} + \sum_i H_{NV_i-target} + \sum_i H_{NV_i-bath}. \quad (1)$$

where the first three terms denote the Hamiltonians of the isolated target electron, NV centers and the nuclear spin bath respectively, and the last three terms represent the interaction between different NV centers, the coupling of the NV centers to the target electron spin, and the coupling of the NV centers to the nuclear spin bath in diamond. Here, we assume the Hamiltonian of the NV center is as follows^{21,22}

$$H_{NV_i} = \Delta_i (S_i^z)^2 + \varepsilon_i [(S_i^x)^2 - (S_i^y)^2] - \frac{\gamma_e}{2\pi} \mathbf{B} \cdot \mathbf{S}_i. \quad (2)$$

where Δ_i and ε_i denote the zero-field splitting and the strain-induced transverse anisotropy for the i th NV center respectively, $\gamma_e = 17.6 \mu\text{s}^{-1} \text{ Gauss}^{-1}$ is the electron gyromagnetic ratio and \mathbf{B} is the magnetic field. With a magnetic field applied along the $[111]$ axis (denoted as z axis), the NV center has three spin eigenstates ($|+1\rangle, |0\rangle, |-1\rangle$) quantized along the NV axis if there is no transverse anisotropy. However, the introduction of the transverse anisotropy breaks the degeneracy of the $|\pm 1\rangle$ states even in zero field (the eigenstate $|0\rangle$ is almost unperturbed since $\Delta_i \gg \varepsilon_i$) and results in renormalized eigenstates $|\alpha\rangle$ and $|\beta\rangle$.²³ In the new eigenstate basis of the i th NV center, the full Hamiltonian in Eq. (1) can be recast as

$$H \approx H_R (|\alpha\rangle_i \langle\alpha| - |\beta\rangle_i \langle\beta|) + H_0, \quad (3)$$

with

$$H_R \approx (\varepsilon_i^2 + \omega^2)^{1/2} + (\varepsilon_i^2 + \omega^2)^{-1/2} [\omega(h_T + h_B + h_N) + (h_T + h_B + h_N)^2/2], \quad (4)$$

$$H_0 = H_{target} + \sum_{j,k \neq i} H_{NV_j-NV_k} + \sum_{j \neq i} (H_{NV_j} + H_{NV_j-bath}) + H_{bath}, \quad (5)$$

where H_R denotes one part of the Hamiltonian conditioned on the the i th NV center, H_0 denotes the other part of the Hamiltonian independent of the state of the i th NV center, $\omega = \gamma_e B_z / 2\pi$ is the Zeeman frequency of the NV center, $h_T = (\hat{\mathbf{z}} \cdot \mathbb{A}) \cdot \mathbf{S}_0$ is the magnetic field produced by the target electron spin, $h_N = \sum_{j \neq i} (\hat{\mathbf{z}} \cdot \mathbb{A}_j) \cdot \mathbf{S}_j$ is the magnetic field produced by the other NV centers, $h_B = \sum_m (\hat{\mathbf{z}} \cdot \mathbb{B}_m) \cdot \mathbf{I}_m$ is the nuclear Overhauser field for the i th NV center due to the hyperfine interaction with the nuclear spin bath, and $H_{bath} = -\frac{\gamma_n}{2\pi} \mathbf{B} \cdot \sum_m \mathbf{I}_m + \sum_{m < n} \mathbf{I}_m \cdot \mathbb{D}_{mn} \cdot \mathbf{I}_n$ denotes the dipolar interaction among nuclear spins, $\mathbb{A}_m / \mathbb{B}_j / \mathbb{D}_{mn}$ denotes the electron-electron, electron-nuclear and nuclear-nuclear dipolar interaction tensors respectively, and γ_e / γ_n are the gyromagnetic ratios of the electron/nuclear spins.

As shown in Eq.(4), the renormalized eigenstates $\{|\alpha\rangle_i, |\beta\rangle_i\}$ have eigenenergies $\pm(\epsilon_i^2 + \omega^2)^{1/2}$. The dipolar interaction between the NV centers and the target spin, the hyperfine interaction between the NV centers and the nuclear spin bath and the dipolar interaction between different NV centers are renormalized up to a factor of $\omega(\epsilon_i^2 + \omega^2)^{-1/2}$ in the first order. The second-order term has a large contribution to the nuclear spin bath dynamics in weak magnetic field and should be considered in the calculations. In this paper we consider the single transition ($|0\rangle \leftrightarrow |\alpha\rangle_i$).

The NV center spin decoherence in high-purity diamond is mainly caused by the hyperfine interaction with the ^{13}C nuclear spins.^{24,25} At finite temperature, the random orientations of the nuclear spins result in local field fluctuation (thermal fluctuation) that can be eliminated by spin echo. The internal dynamics of the spin bath also induces the dynamical quantum fluctuation,²⁴ which cannot be completely removed by dynamical decoupling. To detect a single electron spin by the NV center, we should suppress the thermal and quantum noise caused by the nuclear spin bath while amplifying the effect of the target electron on the NV center spin coherence. The Carr-Purcell-Meiboom-Gill (CPMG) control^{17,26,27} meets both requirements, since it can increase the coherence time of the sensor spin while selectively amplifying the noise at a specific frequency. The target spin can be detected if the sensor spin coherence profile develops characteristic oscilla-

tions caused by the target spin.

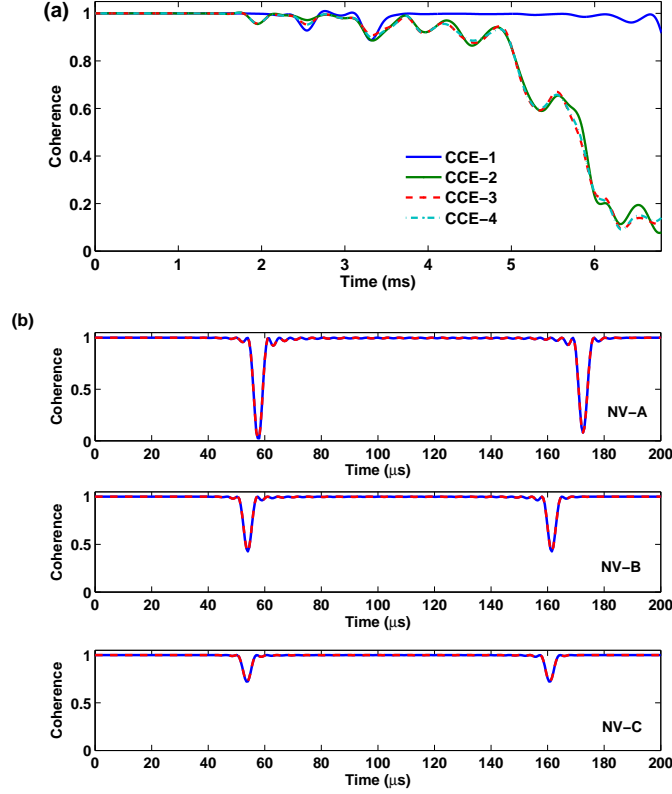


Figure 2: Oscillations caused by the target spin on the NV center spin decoherence with the nuclear spin noise suppressed by dynamical decoupling. (a) Decoherence of a single NV center (in the absence of the target spin and other NV centers) caused by the ^{13}C spin bath with a natural abundance (1.1%) under 30-pulse CPMG control. (b) Spin coherence of three NV centers (with the presence of the target spin) under 30-pulse CPMG control (red dashed lines) which matches the contribution solely from the target electron (blue solid lines) located at ($R_A = 6.13$ nm, $\theta_A = 12.00^\circ$, $R_B = 8.86$ nm, $\theta_B = 45.56^\circ$ and $R_C = 9.96$ nm, $\theta_C = 51.50^\circ$). The NV centers are separated from each other by $6 \sim 7$ nm and the strain-induced transverse anisotropy parameters are $\epsilon_A = \epsilon_B = \epsilon_C = 3$ MHz. A magnetic field $B = 0.1$ Gauss is applied along the NV axis.

The oscillation features in the NV center spin coherence caused by the target spin can be understood as follows. In the classical noise picture, the precession of the single electron spin near the NV sensor gives rise to additional peak structures¹⁷ in the smooth noise spectrum of the nuclear spin bath,²⁸ corresponding to a series of coherence dips in the NV center spin decoherence profile. When the magnetic field is much stronger than the dipolar interaction with the target spin, the peak in the noise spectrum is approximately located at the electron spin Larmor frequency $f_L =$

$\gamma_e B/2\pi$. For N -pulse CPMG control, the coherence dips caused by the target electron spin occur at $t_{dip} = (2k-1)N/(2f_L)$ and the dip depth^{14,28} is $C_{dip} \approx \exp\{-N^2\omega^2(A^\perp)^2/[\gamma_e B^2(\epsilon^2 + \omega^2)]\}$ where A^\perp is the orthogonal component of the dipolar interaction with the target spin.

To detect the target spin with high spatial resolution, the target spins in different positions should have distinguishable fingerprint oscillations imprinted onto the sensor spin coherence. This implies that the applied magnetic field should be comparable to the dipolar interaction between the sensor spin and the target spin. For detecting a single electron spin 5~10 nm away, the magnetic field should be about 0.2~0.05 Gauss. The renormalization factor is about 0.18~0.05 (the strain-induced transverse anisotropy²⁹ ~ 3 MHz), which means the effective dipolar interaction is about ten times smaller than the magnetic field. To increase the detection resolution, we should use the CPMG control with a large number of pulses.

The renormalized dipolar interaction between the i th sensor spin and the target spin has components $[A_R^z, A_R^\perp] = \frac{\mu_0 \gamma_e^2 \omega}{4\pi R^3 \sqrt{\epsilon_i^2 + \omega^2}} [1 - 3\cos^2\theta, 3\sin\theta\cos\theta]$ (where μ_0 is the vacuum permeability) that are determined by the distance R and the zenith angle θ between the displacement and the [111] axis (1b). 1c,d show the different coherence oscillations, from which we can see that an atomic-scale change of the position of the target spin would have noticeable influence on the time-domain coherence features of the NV center spin. It is worth noting that the contour plot in 1c is mirror symmetric about the $\theta = \pi/2$ line owing to the symmetry of the dipolar interaction. We may use the coherence features to determine the distance and zenith angle of the target spin.

To fully determine the three-dimensional position of the target spin, we propose to use multiple NV centers as the sensor spins, in analogue to the multi-satellite global positioning systems. We consider three NV sensor spins (A, B, C) embedded near the surface of a diamond tip. The three NV centers can be separately addressed by their different zero-field splittings (~ 7 MHz) due to the difference in the strain-induced symmetry breaking that usually occurs in real diamond.²⁹ In the simulation, we assume the zero-field splittings of the three NV centers to be $\Delta_A = 2.863$ GHz, $\Delta_B = 2.870$ GHz and $\Delta_C = 2.877$ GHz. The differences in the zero-field splittings also help suppress the exchange interaction between the NV center spins in the multi-spin sensor, which

simplifies the data analysis for the positioning. We may use the CPMG control with a specific frequency to induce the spin transition in one NV center while leaving the states of the other NV centers unchanged. We get three sets of coordinates $(R_A, \theta_A), (R_B, \theta_B), (R_C, \theta_C)$ by comparing the coherent oscillations due to the target spin with the dip features in the spin decoherence of the three NV centers. Therefore the three-dimensional coordinates of the target spin are determined.

For simplicity we suppose the three NV centers are all along the crystal axis [111]. The NV centers are separated from each other by $6 \sim 7$ nm (so that the dipolar interaction between them is less than \sim MHz). The differences between the zero-field splittings are much stronger than the dipolar interaction between different NV centers. As a result, the flip-flops between the NV center spins are negligible.¹⁷ Therefore we can consider the pure dephasing of the sensor spins.

We solve the pure dephasing problem with inclusion of the interactions between the NV centers, the coupling to the target electron spin, and the coupling to the nuclear spin bath, by adopting the well-established cluster-correlation expansion method (CCE).^{24,30,31} The key idea is that the qubit coherence can be expressed as the product of cluster correlations. In real calculations, it often suffices to truncate the expansion up to the minimum size M of the clusters (CCE- M) to get converged results. It is clear from 2a that the spin coherence of a single NV center in ^{13}C nuclear spin bath with a natural abundance 1.1% can be well protected for $t < 1.6\text{ms}$ under 30-pulse CPMG control. In recent experiments, stable and well-behaved NV centers located with depth ranging from 1 to 10 nm from the diamond surface have been observed and the dephasing time T_2 longer than $100\mu\text{s}$ has been achieved for the depth of 5 nm from the diamond surface.^{32,33} The coherence time of the NV electron spin near surface can be further increased by high temperature annealing.³⁴ As shown in 1c,d, the typical timescale of the fingerprint oscillation of a target spin is much shorter than the NV electron spin coherence time, so the nuclear spin bath would have negligible effect on the positioning. The interactions between the NV centers also have negligible influence on the spin coherence due to the different zero-field splittings,²⁴ therefore the spin coherence of the NV centers matches the contribution solely from the target electron spin (2b).

3 shows the numerical simulation for positioning a target spin. First, we establish a fingerprint

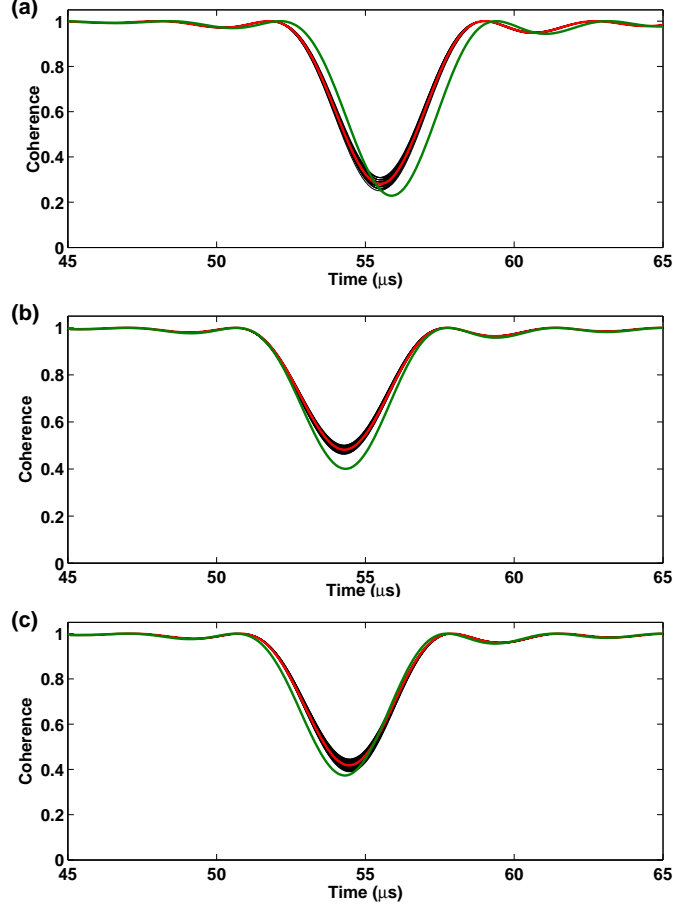


Figure 3: Numerical simulation for positioning a target spin. The red lines represent the spin coherence obtained from the detection while the black solid lines represent the matched oscillation patterns in the fingerprint library (the discrete steps are taken as $dR = 0.02$ nm, $d\theta = 0.2^\circ$ here). The position and depth of the first dip in the spin coherence oscillations are used as the criteria for matching. The estimated locations of the electron relative to the three NV centers are (a) $R_A \in [7.43 \sim 7.53$ nm], $\theta_A \in [19.6 \sim 20.6^\circ]$, (b) $R_B \in [8.82 \sim 8.94$ nm], $\theta_B \in [35.2 \sim 36.2^\circ]$ and (c) $R_C \in [8.56 \sim 8.67$ nm], $\theta_C \in [32.6 \sim 33.8^\circ]$. The exact position of the target spin is such that $R_A = 7.49$ nm, $\theta_A = 20.29^\circ$, $R_B = 8.91$ nm, $\theta_B = 35.69^\circ$ and $R_C = 8.63$ nm, $\theta_C = 33.03^\circ$. The green lines represent the oscillation patterns if the target spin is moved about 0.6 nm away from its original position.

library to store the positions and depths of the dips or peaks in the decoherence patterns caused by a single electron spin located in a large range ($5 \text{ nm} \leq R \leq 30 \text{ nm}$, $0 \leq \theta \leq \pi/2$). R and θ are discretized with resolution $dR=0.02 \text{ nm}$ and $d\theta=0.2^\circ$. Second, we put the diamond tip containing three NV centers close to the target spin and get the respective spin coherence profiles of the three NV centers under 30-pulse CPMG control. Third, by matching the sensor spin coherence oscillations to the fingerprint library, the position of the target spin is restricted to a small spatial region intersected by the small ranges of the three sets of parameters (R_i, θ_i) . The smaller the volume of the intersected region, the higher the resolution in detecting the target spin. In the simulation, the resolution of less than 0.1 nm is achieved.

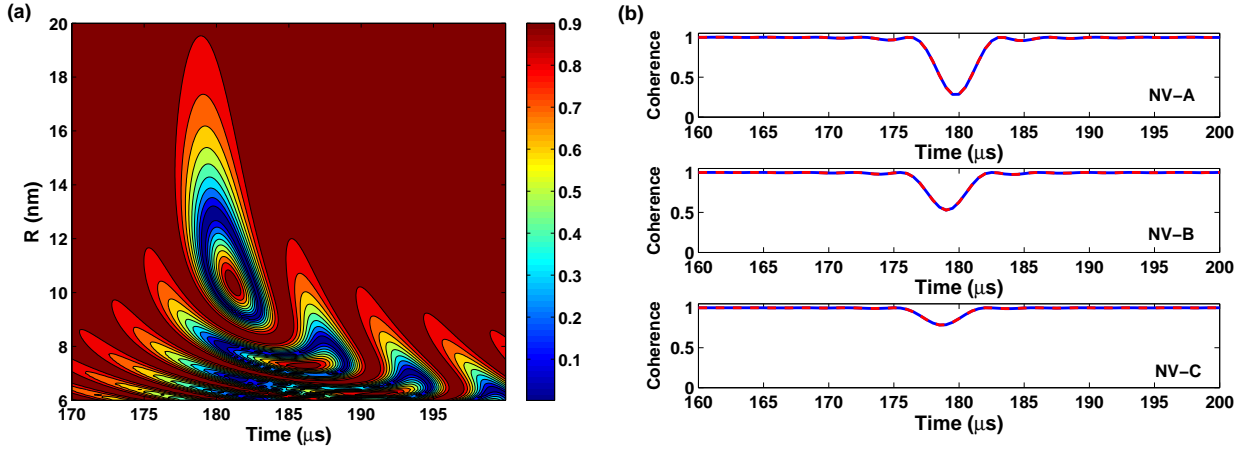


Figure 4: Positioning of a single spin about 20 nm away. (a) NV center spin decoherence caused solely by the target spin under 50-pulse CPMG control as a function of time and the distance R with a zenith angle $\theta = \pi/3$. (b) Spin coherence of three NV centers under 100-pulse CPMG control (red dashed lines) which matches the contribution solely from a single electron spin (blue solid lines) located at $(R_A = 13.61 \text{ nm}, \theta_A = 28.28^\circ, R_B = 15.49 \text{ nm}, \theta_B = 38.09^\circ, R_C = 17.90 \text{ nm}, \theta_C = 47.07^\circ)$. The strain-induced transverse anisotropy parameters are $\epsilon_A = \epsilon_B = \epsilon_C = 2 \text{ MHz}$ and a magnetic field $B = 0.1 \text{ Gauss}$ is applied along the NV axis.

Now we discuss how to extend the detection range of a target spin. The strain-induced transverse anisotropy of the NV center leads to zero-field splitting of the $|\pm 1\rangle$ states and the renormalized eigenstates $\{|\alpha\rangle, |\beta\rangle\}$ have a smaller effective magnetic moment. Consequently, the decoherence caused by the target spin would be suppressed, which is disadvantageous to the positioning. To increase the detection range, the strain-induced transverse anisotropy should be decreased. The

dipolar interaction between the NV sensor spin and the target spin decreases rapidly as the distance between them increases. The magnetic field should be decreased correspondingly to be comparable to the interaction between the sensor spin and target spin. However, the renormalized dipolar interaction decreases almost linearly with the magnetic field. Therefore, the detection range cannot be increased by decreasing the magnetic field. In this case, we can increase the number of CPMG pulses to further amplify the effect of slight difference of the dipolar interaction on the time and depth of the coherence dip. As shown in 4, under 100-pulse CPMG control, the detection range of the multi-spin sensor can be extended to ~ 20 nm. At such a large distance, we can still achieve a resolution as high as 0.3 nm in the simulation.

In conclusion, we have proposed and numerically demonstrated that atomic-scale positioning of single electron spins can be achieved by using multiple NV centers as the sensor. Each NV sensor spin works independently and gathers information about the spatial range of the target spin. By integrating the information provided by multiple NV sensor spins, the position of the target can be accurately determined. The scheme, without requiring spatial scanning or varying the magnetic field, provides an approach to fast positioning of single spins with sub-nanometer resolution.

Acknowledgement

This work was supported by HongKong RGC/GRF CUHK402410, the CUHK Focused Investments Scheme, Hong Kong RGC/CRF HKU8/CRF/11G, National Basic Research Program of China (973 Program) under Grant No. G2009CB929300 and National Natural Science Foundation of China under Grant No. 61121491.

References

- (1) Nair, R. R.; Sepioni, M.; Tsai, I.-L.; Lehtinen, O.; Keinonen, J.; Krashennnikov, A. V.; Thomson, T.; Geim, A. K.; Grigorieva, I. V. *Nature Phys.* **2012**, 8, 199.
- (2) Martin Y.; Wickramasinghe, H. K. *Appl. Phys. Lett.* **1987**, 50, 1455.

- (3) Hubbell, W. L.; Cafiso, D. S.; Altenbach, C. *Nature Struct. Biol.* **2000**, 7, 735.
- (4) Rugar, D.; Budakian, R.; Mamin H. J.; Chui, B. W. *Nature* **2004**, 430, 329.
- (5) Grinolds, M. S.; Maletinsky, P.; Hong, S.; Lukin, M. D.; Walsworth, R. L.; Yacoby, A. *Nature Phys.* **2011**, 7, 687.
- (6) Jelezko, F.; Gaebel, T.; Popa, I.; Domhan, M.; Gruber, A.; Wrachtrup, J. *Phys. Rev. Lett.* **2004**, 93, 130501.
- (7) Gaebel, T.; Domhan, M.; Popa, I.; Wittmann, C.; Neumann, P.; Jelezko, F.; Rabeau, J. R.; Stavrias, N.; Greentree, A. D.; Prawer, S.; Meijer, J.; Twamley, J.; Hemmer, P. R.; Wrachtrup, J. *Nature Phys.* **2006**, 2, 408.
- (8) Childress, L.; Dutt, M. V. G.; Taylor, J. M.; Zibrov, A. S.; Jelezko, F.; Wrachtrup, J.; Hemmer, P. R.; Lukin, M. D. *Science* **2006**, 314, 281.
- (9) Robledo, L.; Childress, L.; Bernien, H.; Hensen, B.; Alkemade, P. F. A.; Hanson, R. *Nature* **2011**, 477, 574.
- (10) Lenef, A.; Rand, S. C. *Phys. Rev. B* **1996**, 53, 13441.
- (11) Hanson, R.; Mendoza, F. M.; Epstein, R. J.; Awschalom, D. D. *Phys. Rev. Lett.* **2006**, 97, 087601.
- (12) Balasubramanian, G.; Neumann, P.; Twitchen, D.; Markham, M.; Kolesov, R.; Mizuochi, N.; Isoya, J.; Achard, J.; Beck, J.; Tissler, J.; Jacques, V.; Hemmer, P.; Jelezko, F.; Wrachtrup, J. *Nature Mat.* **2009**, 8, 383.
- (13) Maletinsky, P.; Hong, S.; Grinolds, M. S.; Hausmann, B.; Lukin, M. D.; Walsworth, R. L.; Loncar M.; Yacoby, A. *Nature Nanotech.* **2012**, 7, 320.
- (14) Zhao, N.; Honert, J.; Schmid, B.; Klas, M.; Isoya, J.; Markham, M.; Twitchen, D.; Jelezko, F.; Liu, R. B.; Fedder H.; Wrachtrup, J. *Nature Nanotech.* **2012**, 7, 657.

- (15) Taminiau, T. H.; Wagenaar, J. J. T.; van der Sar, T.; Jelezko, F.; Dobrovitski, V. V.; Hanson, R. *Phys. Rev. Lett.* **2012**, 109, 137602.
- (16) Kolkowitz, S.; Unterreithmeier, Q. P.; Bennett, S. D.; Lukin, M. D. *Phys. Rev. Lett.* **2012**, 109, 137601.
- (17) Zhao, N.; Hu, J. -L.; Ho, S. -W.; Wan T. K.; Liu, R. B. *Nature Nanotech.* **2011**, 6, 242.
- (18) Grinolds, M. S.; Hong, S.; Maletinsky, P.; Luan, L.; Lukin, M. D.; Walsworth, R. L.; Yacoby, A. arXiv: 1209. 0203v1.
- (19) Viola, L.; Knill, E.; Lloyd, S. *Phys. Rev. Lett.* **1999**, 82, 2417.
- (20) Pham, L. M.; Bar-Gill, N.; Belthangady, C.; Le Sage, D.; Cappellaro, P.; Lukin, M. D.; Yacoby, A.; Walsworth, R. L. *Phys. Rev. B* **2012**, 86, 045214.
- (21) Dolde, F.; Fedder, H.; Doherty, M. W.; Nöbauer, T.; Rempp, F.; Balasubramanian, G.; Wolf, T.; Reinhard, F.; Hollenberg, C. L.; Jelezko, F.; Wrachtrup, J. *Nature Phys.* **2011**, 7, 459.
- (22) Vanoort, E.; Glasbeek, M. *Chem. Phys. Lett.* **1990**, 168, 529.
- (23) Yang, W.; Liu, R. B. *Phys. Rev. B* **2008**, 77, 085302.
- (24) Zhao, N.; Ho, S. -W.; R. -W. Ho; Liu, R. B. *Phys. Rev. B* **2012**, 85, 115303.
- (25) Zhao, N.; Wang, Z. -Y.; Liu, R. B. *Phys. Rev. Lett.* **2011**, 106, 217205.
- (26) de Lange, G.; Wang, Z. H.; Risté, D.; Dobrovitski V. V.; Hanson, R. *Science* **2010**, 330, 60.
- (27) Ryan, C.; Hodges J.; Cory, D. *Phys. Rev. Lett.* **2010**, 105, 200402.
- (28) Cywiński, Ł.; Lutchyn, R.; Nave, C.; Das Sarma, S. *Phys. Rev. B* **2008**, 77, 174509.
- (29) Gruber, A.; Dräbenstedt, A.; Tietz, C.; Fleury, L.; Wrachtrup, J.; von Borczyskowski, C. *Science* **1997**, 276, 2012.

- (30) Yang, W.; Wang, Z. Y.; Liu, R. B. *Front. Phys.* **2011**, 6, 2.
- (31) Yang W.; Liu, R. B. *Phys. Rev. B* **2008**, 78, 085315.
- (32) Ohno, K.; Heremans, F. J.; Bassett, L. C.; Myers, B. A.; Toyli, D. M.; Jayich, A. C. B.; Palmstrøm, C. J.; Awschalom, D. D. *Appl. Phys. Lett.* **2012**, 101, 082413.
- (33) Ofori-Okai, B. K.; Pezzagna, S.; Chang, K.; Loretz, M.; Schirhagl, R.; Tao, Y.; Moores, B. A.; Groot-Berning, K.; Meijer, J.; Degen, C. L. *Phys. Rev. B* **2012**, 86, 081406.
- (34) Naydenov, B.; Reinhard, F.; Lämle, A.; Richter, V.; Kalish, R.; D’Haenens-Johansson, U. F. S.; Newton, M.; Jelezko, F.; Wrachtrup, J. *Appl. Phys. Lett.* **2010**, 97, 242511.